Crystallization Kinetics of GeSbTe Phase-Change Nanoparticles Resolved by Ultrafast Calorimetry

Chen, Bin; Brink, ten, Gert; Palasantzas, Georgios; Kooi, Bart J.

Published in:
The Journal of Physical Chemistry. C: Nanomaterials and Interfaces

DOI:
10.1021/acs.jpcc.6b11707

Publication date:
2017

THE JOURNAL OF PHYSICAL CHEMISTRY C

Article

pubs.acs.org/JPCC

Crystallization Kinetics of GeSbTe Phase-Change Nanoparticles Resolved by Ultrafast Calorimetry

Bin Chen, Gert H. ten Brink, George Palasantzas, and Bart J. Kooi*

Zernike Institute for Advanced Materials, University of Groningen, Nijenborgh 4, 9747AG Groningen, The Netherlands

Supporting Information

ABSTRACT: Although nanostructured phase-change materials (PCMs) are considered as the building blocks of next-generation phase-change memory and other emerging optoelectronic applications, the kinetics of the crystallization, the central property in switching, remains ambiguous in the high-temperature regime. Therefore, we present here an innovative exploration of the crystallization kinetics of $Ge_2Sb_2Te_5$ (GST) nanoparticles (NPs) exploiting differential scanning calorimetry with ultrafast heating up to 40 000 K s^{-1}. Our results demonstrate that the non-Arrhenius thermal dependence of viscosity at high temperature becomes an Arrhenius-like behavior when the glass transition is approached, indicating a fragile-to-strong (FS) crossover in the as-deposited amorphous GST NPs. The overall crystal growth rate of the GST NPs is unraveled as well. This unique feature of the FS crossover is favorable for memory applications as it is correlated to improved data retention. Furthermore, we show that methane incorporation during NP production enhances the stability of the amorphous NP phase (and thereby data retention), while a comparable maximum crystal growth rate is still observed. These results offer deep insight into the crystallization kinetics of nanostructured GST, paving the way for designing nonvolatile memories with PCM dimensions smaller than 20 nm.

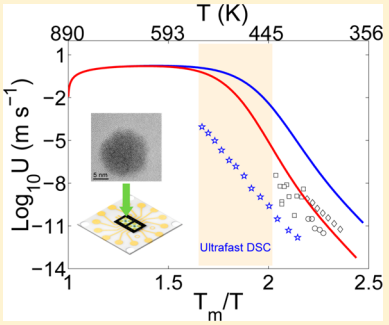

INTRODUCTION

$Ge_2Sb_2Te_5$ (GST), one of the prototypical phase-change materials (PCMs), enables rapid and reversible switching between its amorphous and crystalline phases, which is accompanied by large optical and electrical contrast. This unique feature makes GST attractive for data-storage applications[1−3] and a strong contender for emerging applications, such as solid-state displays,[4] optical modulators,[5] neuromorphic computing,[6,7] on-chip photonic circuitry,[8] and plasmonic-based circuits.[9] Crystallization lies at the heart of the switching in phase-change technology; thus, a solid understanding of the crystallization kinetics entails a crucial aspect of designing phase-change memory.

Conventional measurements are only able to investigate crystallization kinetics within a relatively low temperature range (near the glass transition temperature).[10−13] However, in actual applications, crystallization generally takes place at higher temperatures. Despite its scientific and technologic relevance, the analysis of the crystallization kinetics at these high temperatures has remained for a long time highly challenging due to the ultrashort time and length scales (ns and nm) involved. This situation persisted until very recently, where ultrafast differential scanning calorimetry (DSC) was utilized to explore the crystallization process of GST films with heating rates up to 40 000 K s^{-1}.[14] Using subsequent extensive modeling, growth rates ranging from the glass transition temperature to the melting temperature were derived for the film structures, showing a remarkable breakdown of Arrhenius behavior in the viscosity at heating rates beyond ∼500 K s^{-1}. Non-Arrhenius thermal dependence of the viscosity at high temperatures has lately been widely observed in both nucleation-dominated and growth-dominated PCMs. For instance, for GST confined in memory cells it was demonstrated that non-Arrhenius thermal dependence of crystallization at high temperatures crosses over to a wide temperature range at lower temperatures where still Arrhenius behavior prevails.[15−17] In recent years, also for other PCMs, such as GeTe films,[18] supercooled and melt-quenched AgInSbTe films,[19−21] and GeSb films,[22,23] the crystallization kinetics have been determined based on nonconventional techniques with measurements spanning relatively wide temperature ranges. All these works confirm the breakdown of Arrhenius dependence for amorphous PCMs at high temperatures. However, a question that remains is whether this breakdown can be described on the basis of a model for viscosity with a single value for the fragility.

In parallel, down-scaling the GST into (sublithographic) nanostructures generates tremendous advantages for PCM-based memory including ultrafast switching, low switching power, and ultrahigh density. Therefore, many efforts have been devoted to enter this promising field.[24,25] In this context, the fabrication of monodisperse GST nanoparticles (NPs) with good size and composition control has been a great challenge for a long time. We achieved a breakthrough by exploiting a technique based on gas-phase condensation and magnetron sputtering, which is capable of meeting the requirements of

Received: November 21, 2016
Revised: March 31, 2017
Published: April 5, 2017

DOI: 10.1021/acs.jpcc.6b11707
J. Phys. Chem. C 2017, 121, 8569−8578

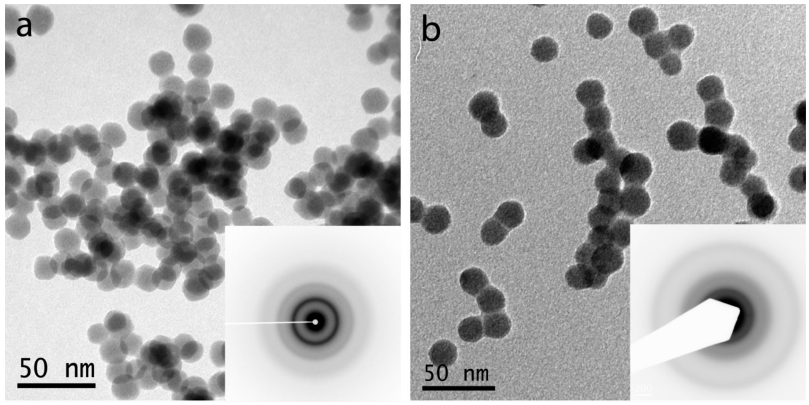

Figure 1. Morphology of $Ge_2Sb_2Te_5$ (GST) nanoparticles (NPs). (a), (b) Bright-field image of the GST NPs produced with H_2 (NPs (H_2)) and CH_4 (NPs (CH_4)), respectively. The average diameters of the NPs in these two samples are 16.0 ± 1.3 and 16.8 ± 1.7 nm, respectively. Insets show the selected area electron diffraction patterns of the corresponding NPs, clearly demonstrating the amorphous nature of the as-deposited NPs.

GST NP fabrication.[26] Size-dependent crystallization was observed through *in situ* heating in a transmission electron microscope. Yet this previous work mainly focused on the crystallization at relatively low temperatures because of the limitation inherent to the *in situ* TEM heating method. Therefore, the crystallization kinetics of GST NPs remains unknown for the high-temperature regime. In this manuscript we present a facile method to synthesize size- and composition-controlled $Ge_2Sb_2Te_5$ nanoparticles via gas-phase condensation, followed by the unprecedented exploration of crystallization kinetics of GST NPs via ultrafast DSC. By varying the heating rate more than 3 orders of magnitude, the temperature-dependent viscosity and growth rate of the crystallization have been unraveled, providing evidence for a fragile-to-strong crossover in as-deposited amorphous GST NPs. Moreover, it is shown that methane addition during NP production is advantageous for application of NPs in PCM-based devices due to the fact that it increases the amorphous phase stability near the glass transition temperature, whereas the maximum switching speed at high temperature is not reduced.

EXPERIMENTAL METHODS

GeSbTe Nanoparticle Synthesis. The $Ge_2Sb_2Te_5$ (GST) nanoparticles (NPs) were directly deposited on a precleaned glass substrate without capping layer, utilizing a home-modified nanocluster system Nanogen50 from Mantis Deposition Ltd. The substrate was put close to the aperture of the aggregation chamber in order to synthesize a large amount of NPs. The main chamber (to collect the NPs) is evacuated to a pressure of 10^{-8} mbar. Amorphous GST NPs were directly synthesized by sputtering the GST target (purity of 99.99%), employing a low current (0.105 A) to avoid the formation of crystalline NPs. The Ar gas flow (purity 99.9999%) used for the two types of samples analyzed in the present work is 35 sccm, with H_2/CH_4 (purity 99.99%) as extra gas to facilitate the development of nascent clusters in the plasma. In this manuscript, we show the ability of preparing nanoparticles with a large yield, as shown in the Figure S1 in Supporting Information (SI). The morphology of the as-deposited NPs was subsequently characterized by transmission electron microscopy (JEOL 2010) at 200 kV. The composition of the NPs was characterized by energy-disperse X-ray spectrometry (Thermo Instruments) attached to the TEM, as shown in Figure S2 of the SI.

Ultrafast Differential Scanning Calorimetry Measurement. The phase transitions of the samples were subsequently measured by ultrafast differential scanning calorimetry (DSC, Mettler-Toledo Flash DSC 1), with the sensor chips (USF-1) each containing the actual sensor and reference area. The GST NPs were scraped off from the glass substrate and then were deposited on the effective area of the chip sensor. Instead of the loose powder/multiflakes we used for Ge−Sb PCMs, a single planar flake consisting of GST NPs parallel to the sensor surface was adopted here to run the measurements. The approximate area that was subjected to ultrafast heating is roughly 60 × 60 μm^2 and 20 × 20 μm^2 for NPs (H_2) and NPs (CH_4), respectively. This methodology remarkably increases the thermal contact between the materials and the chip sensor, as shown in Figure S3 of the SI with much less scattering of the crystallization temperature in the Kissinger plot. Actually, our results show that all previously published ultrafast DSC work employing loose powder or multiflakes (of PCMs) can contain erroneous results for the higher heating rate (and thus temperature) regime. The heating rates (Φ) adopted in this manuscript vary from 10 to 40 000 K s^{-1}. At each Φ, measurements were repeated at least 3 times for low Φ and 5−10 times for high Φ, as the values of the crystallization temperature become more scattered. Thermal lag and temperature calibration of the Flash DSC are discussed in detail in Section 2 of the SI.

Numerical Modeling. Similar to our previous work,[23] numerical modeling utilizing JMAK theory has been performed to interpret the data from the ultrafast DSC measurements. The viscosity model (MYEGA model) we employed successfully for the Ge−Sb alloy turned out inadequate to explain the Arrhenius behavior persisting for such a large temperature range in the Kissinger plot presented in the present work. Therefore, the generalized MYEGA model was adopted for the fitting.[27] Note that in all the fittings performed in this manuscript the fractional Stokes−Einstein relation between viscosity and growth rate has been used, with ξ = 0.65 suggested by previous work.[14] The details of JMAK modeling can be found in the SI of our previous work.[23] For this JMAK model, descriptions of nucleation and growth are required. For the description of nucleation it is assumed that it is independent of time and temperature; i.e., we assume a constant nuclei density (site saturation), analogous to what was adopted for the modeling of GST films.[14] However, in the SI of the present work, we show that the results hardly change when

DOI: 10.1021/acs.jpcc.6b11707
J. Phys. Chem. C 2017, 121, 8569−8578

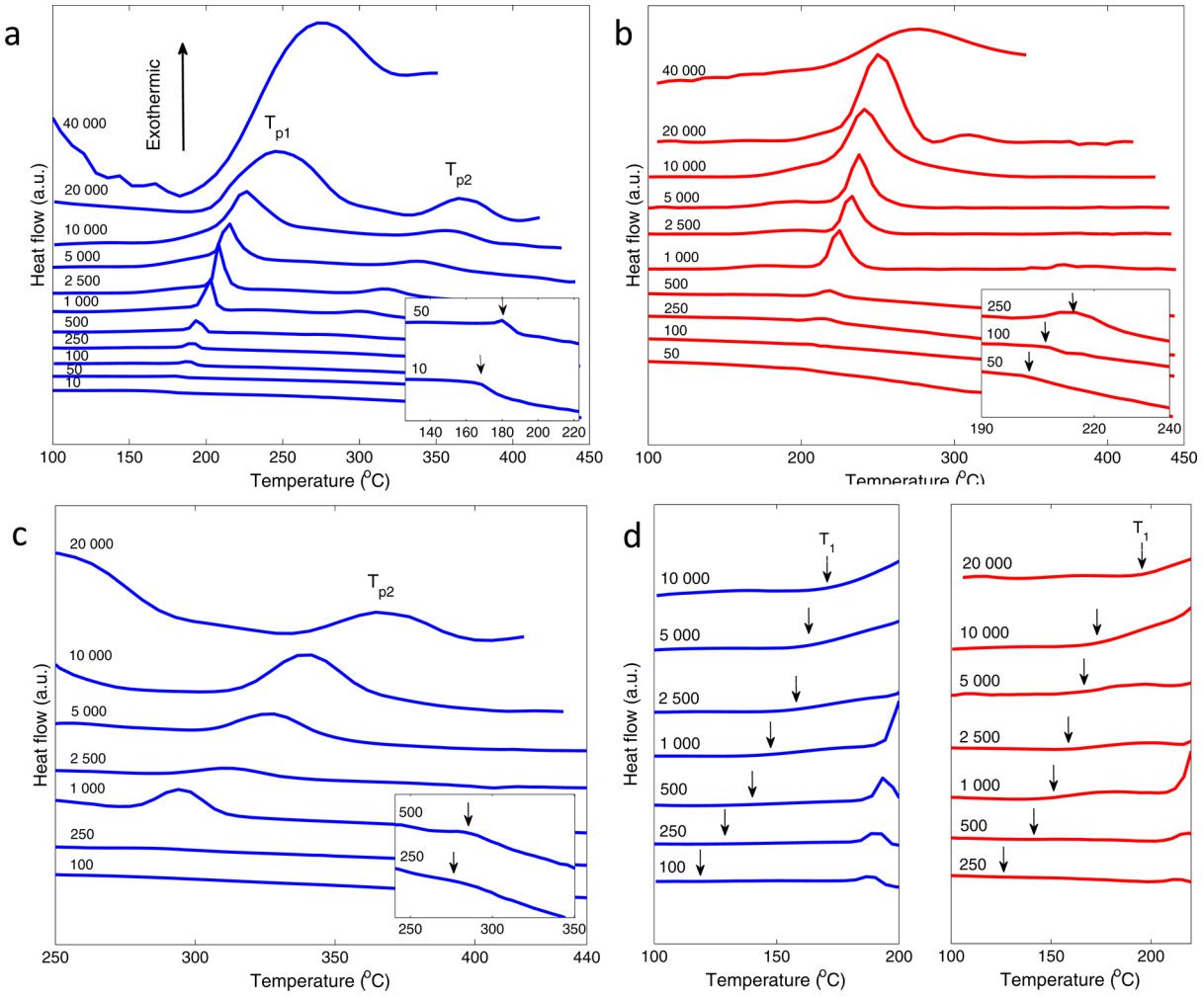

Figure 2. Ultrafast DSC traces for GST NPs. (a), (b) Ultrafast DSC traces for GST NPs (H_2) and NPs (CH_4), respectively, for heating rates (Φ) ranging from 10 to 40 000 K s^{-1}. Insets of (a) and (b) show the close-up of the crystallization peaks at lower Φ. (c) Zoomed-in ultrafast DSC traces of rock-salt to rhombohedral structural transition in NPs (H_2) at Φ ranging from 250 to 20 000 K s^{-1}. (d) Evolution of the structural relaxation temperatures with Φ for NPs (H_2) and NPs (CH_4). The blue and red curves in the figures hold for NPs (H_2) and NPs (CH_4), respectively.

we adopt a more intricate steady-state nucleation model. For the description of the growth (rate) eq 2 has been used, in which the viscosity is described by the generalized MYEGA model.

Apart from the ultrafast DSC data presented in the Kissinger plot, also two relevant data points, one for GST NPs (H_2) and one for GST NPs (CH_4), were added for very low heating rates Φ (0.03 K s^{-1}) based on our previous in situ TEM work.[26] The data point for GST NPs (H_2) is reliable, but it is not precise for GST NPs (CH_4). The reason is that it is hard to accurately control for different sample batches the amount of methane incorporated in the gas phase during the NP sample production. Therefore, this single data point for GST NPs (CH_4) in the Kissinger plot is not used when fitting the JMAK-based model to the experimental data.

RESULTS AND DISCUSSION

Morphology and Size Distribution. Size-dependent crystallization has been observed for $Ge_2Sb_2Te_5$ (GST) nanoparticles (NPs),[26] where the size, morphology, structure, and crystallization temperature of the as-deposited NPs have been characterized by transmission electron microscopy (TEM). As shown in Figure 1, relatively monodisperse GST NPs have been synthesized, with average diameters of 16.0 ± 1.3 and 16.8 ± 1.7 nm for NPs synthesized with either H_2 or CH_4 added to the base Ar gas, hereafter named NPs (H_2) and NPs (CH_4). Detailed size distributions of these two samples can be found in Figure S4 of the Supporting Information (SI). The similar sizes and narrow size distribution of the two GST NP (CH_4) and (H_2) samples exclude size effects on the crystallization observed in the present work. Although the NPs were produced with a relatively high coverage, they are not coalesced but only aggregated, as can be seen clearly in Figure 1. The spherical morphology is an indication of the amorphous nature of the NPs, which is further confirmed by selected area electron diffraction (SAED). As manifested by the insets of Figure 1, the SAED patterns demonstrate that the NPs are amorphous due to the lack of sharp crystalline rings. The composition of these NPs is Ge:Sb:Te = 19:24:57 (±1) at.%, as determined by energy-dispersive X-ray spectrometry; see the spectrum in Figure S2 of the SI. Note that the TEM grids were located at the periphery of the NP cluster beam during production, retaining a lower coverage in comparison to the center part; see the large amount of NPs in Figure S1 of the SI. High yield synthesis of GST NPs has been achieved by gas-phase condensation in order to obtain a good signal-to-noise

DOI: 10.1021/acs.jpcc.6b11707
J. Phys. Chem. C 2017, 121, 8569−8578

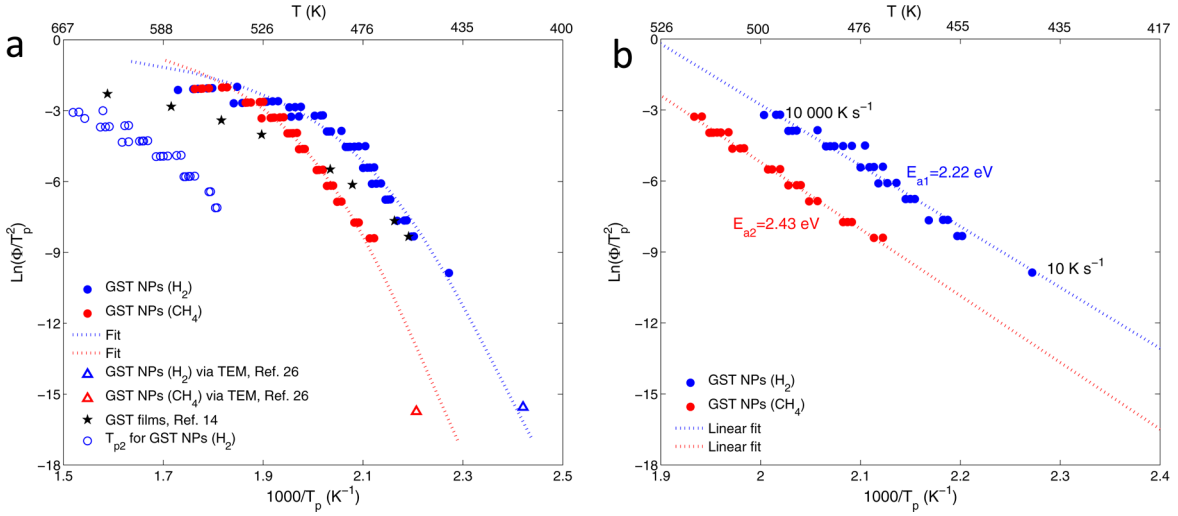

Figure 3. Kissinger plot with optimized model fits to the data. (a) Kissinger plot for NPs (H_2) and NPs (CH_4). Blue solid circles and blue open circles denote the amorphous to rock-salt transition temperatures (T_{p1}) and rock-salt to rhombohedral transition temperatures (T_{p2}) of NPs (H_2). The red solid circles represent T_{p1} of NPs (CH_4). Dotted lines show the corresponding fits to these data. The black stars show earlier reported T_{p1} of GST films by ultrafast DSC.[14] The blue and red triangles correspond to the T_{p1} of NPs (H_2) and NPs (CH_4), respectively, as obtained using in situ heating in the TEM.[26] (b) Linear fit to the Kissinger plot at lower Φ (up to 10 000 K s^{-1}), leading to crystallization activation energy of 2.22 and 2.43 eV at^{-1} for NPs (H_2) and NPs (CH_4), respectively.

ratio when performing differential scanning calorimetry (DSC) with ultrafast heating. Moreover, we have demonstrated that the NPs do not coalesce during thermal heating in a transmission electron micscope; see the SI of our previous work.[26] Therefore, the above factors enable and ensure the thermal analysis of well-characterized NPs via ultrafast DSC.

Crystallization by Ultrafast DSC. The obtained ultrafast DSC traces for the two GST NP (H_2) and NP (CH_4) samples are shown in Figure 2a,b. The heating rates (Φ) used to obtain the data of the present work vary more than 3 orders of magnitude, from 10 to 40 000 K s^{-1}. Note that a detectable signal of crystallization only appears for Φ beyond 50 K s^{-1} for the NPs (CH_4). The temperatures for the amorphous to rock-salt transition (T_{p1}) drastically increase when higher Φ are applied to both samples; e.g., T_{p1} of NPs (H_2) shifts from 440 at 10 K s^{-1} to 542 K at 40 000 K s^{-1}, as shown in Table S1. Figure 2 also shows that NPs (CH_4) have an (expected) higher T_{p1} than NPs (H_2), particularly at low Φ. For example, T_{p1} for NPs (CH_4) is ∼20 K higher than that of NPs (H_2) at 50 K s^{-1}. In a previous work, we have revealed by *in situ* heating in a TEM that methane addition during GST NP production remarkably increase the T_{p1} at relatively low heating rates.[26] Nevertheless, here we observe that this gap of T_{p1} gradually decreases when Φ becomes higher and finally vanishes when Φ reaches 40 000 K s^{-1}. Surprisingly, at high Φ we observe a big divergence in T_{p1} for GST NPs (H_2) compared to GST films as reported in earlier work;[14] see detailed data in Table S1. While the T_{p1}s are very similar at 50 K s^{-1}, the T_{p1} of GST films becomes ∼90 K higher than that of the NPs (H_2) at 40 000 K s^{-1}. This gap can (at least partly) stem from two origins: (1) the thermal lag between the thin film and the ultrafast chip sensor, as is discussed in detail in section 2 of the SI, and (2) it is still very well likely that the kinetics of NPs differs from that of thin films. We did not have the appropriate thin-film samples to verify this, and these tests are beyond the scope of the present work; however, they are of interest for future research.

Furthermore, the rock-salt to trigonal structural transition is also unambiguously observed for the NPs (H_2) in the ultrafast DSC traces when Φ is above 250 K s^{-1}. The signal of this transition is unexpected but intriguing as it was not detected for GST films via ultrafast DSC measurement in previous work.[14] This transition temperature (denoted hereafter as T_{p2}) displays a clear dependence on Φ as well, where it increases when Φ rises, even with a more drastic increment compared to T_{p1}. Locating at around 553 at 250 K s^{-1}, T_{p2} moves to 633 K at 20 000 K s^{-1}, as depicted in Figure 2c. It is noticeable that T_{p2} is invisible in the DSC signal at the lowest Φ because of the small heat release involved compared to the amorphous to rock-salt transition. Interestingly, the rock-salt to trigonal structural transition is unobservable in NPs (CH_4) in the present work (Figure 2b). Several explanations could correlate to this feature: (i) the addition of methane alters T_{p2} to too high temperature which is beyond the upper limit of ultrafast DSC (450 °C); (ii) the incorporation of methane suppresses this structural transition completely; (iii) with methane the transition can still occur but with reduced latent heat (or spread over a larger temperature range) such that it is not detected by the ultrafast DSC. More systematic research is necessary before drawing conclusions on this second transition, and this is out of the scope of the present work. However, the appearance of this specific transition also indicates good thermal contact between the chip sensor and the NP flake, as the heat release involved in this transition is much smaller than that of the amorphous to rock-salt transition. The obtained T_{p2} for GST NPs is much lower than that of the GST films due to the expected strong size dependence of T_{p2}, where it has been observed to reduce sharply with decreasing thickness of GST films.[28]

In the ultrafast DSC traces, a heat release prior to the amorphous to rock-salt transition is also observed, indicated as T_1 in Figure 2d. This exothermic heat flow was ascribed to structural relaxation of the amorphous phase by previous researchers,[29] as the temperature is too low for crystallization. For instance, for GST NPs (H_2) at a heating rate of 100 K s^{-1} the temperature T_1 is 120 °C compared to the crystallization temperature T_{p1} of ∼180 °C. At this T_1 temperature, crystallization only occurs after very long times. For example,

DOI: 10.1021/acs.jpcc.6b11707
J. Phys. Chem. C 2017, 121, 8569−8578

for GST nanowires with a width of 60 nm, the amorphous phase can remain present for ~10^6 s.[24] Therefore, with high heating rate (100 K/s), the heating process from 25 to 125 °C takes only 1 s that is way below the time required to start crystallization at 120 °C. Therefore, no signal for crystallization should be observed at these temperatures indicated by the arrows in Figure 2d. This structural relaxation has been found in other amorphous materials, such as silicon and germanium, and it is attributed to the presence of a spectrum of activation energies for the sites where relaxation takes place.[30,31] For both the GST NP (CH_4) and NP (H_2) samples, T_1 moves toward the onset of the amorphous to rock-salt transition as Φ rises.

Kissinger Analysis. To further understand the crystallization kinetics of the NPs, Kissinger analysis is employed. For crystallization, the activation energy can be obtained using the following equation proposed by Kissinger[32]

$$\frac{Q}{R} = -\frac{d\ln(\Phi/T_p^2)}{d(1/T_p)} \tag{1}$$

with Q being the activation energy for crystallization, R the gas constant, Φ the heating rate, and T_p the peak temperature in the DSC signal. For a crystallization process complying with Arrhenius behavior, the (constant) activation energy can be derived straightforwardly. Figure 3a shows the crystallization data for GST NPs obtained by ultrafast DSC at different Φ, with the blue and red solid circles signifying T_{p1} data for NPs (H_2) and NPs (CH_4), respectively. The single flake methodology (instead of an ensemble of loose flakes) utilized in running the ultrafast heating here effectively improves the thermal contact between the chip sensor and the NP flake, inducing clearly less scatter in T_{p1} in comparison with the employment of loose powder or multiflakes; see more details in Figure S3 of the SI. At low Φ, the Arrhenius behavior is maintained, as indicated by the Kissinger plot (Figure 3). Surprisingly, the Arrhenius behavior for the NPs persists for a considerably larger Φ range (up to 10 000 K s^{-1}) in contrast to GST films previously studied where Arrhenius behavior was reported to break down already at ~500 K s^{-1},[14] as shown Figure 3a by the black stars. It is also observable that NPs (CH_4) have a higher activation energy for crystallization than NPs (H_2) within the Arrhenius behavior range. The Kissinger plot at lower Φ has been zoomed in and linearly fitted (Figure 3b), with an activation energy for crystallization determined as 2.22 and 2.43 eV at^{-1} for NPs (H_2) and NPs (CH_4), respectively. These values coincide well with the reported values for GST films, in a range between 2 and 3 eV by conventional DSC or electrical resistance measurements.[10,33−36] The increase of activation energy induced by CH_4 incorporation is similar to the enhanced activation energy by carbon doping of GST films.[37]

Nevertheless, further increase in Φ (beyond 10 000 K s^{-1}) prompts the breakdown of the Arrhenius behavior, generating a curvature in the Kissinger plot. As a result, the activation energy for crystallization diminishes with the increment of temperature and vanishes at higher temperatures. In order to appropriately interpret these data, Johnson−Mehl−Avrami−Kolmogorov (JMAK) theory has been adopted to fit the Kissinger plot, analogous to our previous work on GeSb alloy.[23] The growth rate of crystallization is vital to utilize the JMAK theory, which can be written as[19]

$$U(T) = \frac{4r_{atom}k_BT}{3\pi\lambda^2 R_{hyd}\eta(T)^{\xi}}\left[1 - \exp\left(-\frac{\Delta G(T)}{k_BT}\right)\right] \tag{2}$$

with $U(T)$ as the growth rate, r_{atom} the atomic radius (~1.5 Å), λ the diffusional jump distance (~2.99 Å), R_{hyd} the hydrodynamic radius ($R_{hyd} = r_{atom}$), k_B the Boltzmann constant, $\eta(T)$ the temperature-dependent viscosity, ξ the decoupling parameter of the Stokes−Einstein equation ($\xi \leq 1$), and $\Delta G(T)$ the change of Gibbs free energy, which can be described, according to Thomson and Spaepen, as[38]

$$\Delta G(T) = \frac{\Delta H_m(T_m - T)}{T_m}\left(\frac{2T}{T_m + T}\right) \tag{3}$$

where ΔH_m is the latent heat of melting, approximately 0.152 eV at^{-1},[39] and T_m is set to 890 K.[16] Note that fractional Stokes−Einstein equation ($U \propto \eta^{-\xi}$ with $\xi \leq 1$) is intrinsically included in eq 2, as the breakdown of Stokes−Einstein relation has been observed in a large number of supercooled glass forming liquids and in particular PCMs and it is attributed to dynamical heterogeneities.[14,40] For the GST NPs we set ξ = 0.65, a value similar to GST films.[14]

An appropriate viscosity model is required to determine the growth rate in eq 2. Although the model proposed by Mauro et al.[41] (MYEGA model hereinafter) provides, as we proved,[23] a much better description of the viscosity of Ge−Sb phase-change materials as compared to the one from Cohen and Grest,[42] it yields inferior fits to the present data for GST NPs owing to its inability to afford Arrhenius behavior in a large temperature range. If the MYEGA model (with a single fragility value) is adopted, it provides very high values of fragility for the NPs (H_2), m = 203, which is higher than the theoretical value for kinetic fragility for glass forming liquids (m = 176).[43] Furthermore, this model leads to very high crystallization temperatures at low heating rates, resulting in a large mismatch to the data obtained by in situ heating in TEM, as shown in Figure S5 of the SI. Furthermore, for NPs (CH_4), it only fits well in the low heating rate range. In contrast, the generalized MYEGA model can avoid all the above problems. Note that the quality of the fits using either the MYEGA model or the Cohen and Grest model remains poor even using more sophisticated models for nucleation instead of the simple constant nuclei density (site saturation) adopted initially. Therefore, we tested a generalized MYEGA model since it enabled a successful description of the complex viscosity in metallic glass-forming liquids[27]

$$\log_{10}\eta(T) = \log_{10}\eta(\infty) + \frac{1}{T\left[W_1\exp\left(-\frac{C_1}{T}\right) + W_2\exp\left(-\frac{C_2}{T}\right)\right]} \tag{4}$$

with $\eta(\infty)$ being viscosity at infinite temperature (here it is taken as 10^{-3} Pa s), T the temperature, and W_1, C_1, W_2, and C_2 the fitting parameters. This model illustrates that two intrinsic terms of viscosity subsist in the liquid, and these two terms can transfer to each other upon cooling or heating. The blue and red dotted curves in Figure 3a denote the modeled Kissinger plots utilizing the generalized MYEGA model (eq 4), showing excellent fits to the corresponding experimental data, with fitting quality evaluated by adjusted R^2 (0.973 and 0.984, respectively). The derived fitting parameters are W_1 = 6921.8, C_1 = 7490.2, W_2 = 6.63 × 10^{-4}, and C_2 = 517.2 for NPs (H_2)

DOI: 10.1021/acs.jpcc.6b11707
J. Phys. Chem. C 2017, 121, 8569−8578

and W_1 = 8259.3, C_1 = 8091.9, W_2 = 5.27 × 10^{-4}, and C_2 = 510.2 for NPs (CH_4). Note that the data become more scattered when Φ becomes high, particularly for Φ above 10 000 K s^{-1}. Therefore, only three data points at the most right side for Φ beyond 10 000 K s^{-1} are weighted to be the most representative data, as they exemplify the best thermal contact between the chip sensor and the NP flake.

Moreover, the evolution of T_{p2} with Φ is also depicted in Figure 3a. A non-Arrhenius behavior is evidently revealed in this figure, inferring a temperature-dependent activation energy for this structural transition. Without a proper growth rate model for this transition, it is currently not possible to model the Kissinger curve via JMAK theory.

Viscosity and Fragility of $Ge_2Sb_2Te_5$ Nanoparticles. Viscosity is of fundamental and practical relevance for glass forming liquids as it is directly associated with the glass transition and relaxation process, indicating the mobility of the atoms, and therefore it is coupled to the growth rate of crystallization. As the unknown parameters in eq 4 have been determined through fitting, the viscosity of the as-deposited amorphous NPs as a function of temperature can be derived straightforwardly; see the red and blue solid curves in the Angell plot of Figure 4, where the temperature-dependent

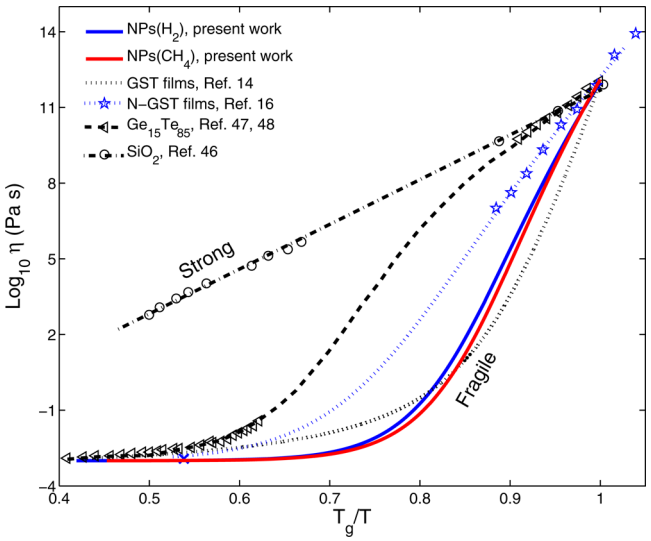

Figure 4. Angell plot for viscosity. The blue and red solid curves represent the modeled viscosity for NPs (H_2) and NPs (CH_4), respectively. The black open circles are the viscosity data for SiO_2 in order to show a strong (undercooled) liquid.[46] The black open triangles and the corresponding fitting curve are the experimental data[47,48] and fitting curve utilizing eq 4 for $Ge_{15}Te_{85}$. The blue stars are the viscosity data for nitrogen-doped GST films,[16] with corresponding fitting curves adopting eq 4. Black dotted curve shows the viscosity for GST films explored by ultrafast DSC.[14]

viscosity of GST films reported previously by Orava et al. is also depicted in comparison (black dotted curve in Figure 4).[14] Unlike the MYEGA model, eq 4 does not directly provide the value of glass transition temperature (T_g) and fragility. Here we set T_g as the temperature at which the viscosity equals 10^{12} Pa s, and then T_g values are determined as 373 and 403 K for NPs (H_2) and NPs (CH_4), respectively. This value for the NPs (H_2) is close to the reported values for the GST films (373–383 K).[14,44] As indicated in a previous work,[26] the crystallization temperature for NPs (H_2) is slightly lower than that of GST films (~10 K), therefore the akin T_g is plausible as the glass transition usually takes place ~10 K lower than T_{p1} at a Φ of 40 K min^{-1} for GST films.[29] The increase of T_g caused by the CH_4 incorporation is ~30 K, which agrees excellently with the rise of T_{p1}, as shown here by the ultrafast DSC measurements and by the *in situ* TEM characterization of our earlier work.[26] The fragility, defined as $m = \left.\frac{d(\log_{10}\eta(T))}{d(T_g/T)}\right|_{T=T_g}$, is determined from the Angell plot for these NPs as well. The fragility of NPs (H_2) is 57, consistent with the value from a previous work (m = 47 for nondoped GST films).[45] Methane addition slightly increases the fragility to a value of 62. These values for fragility are considerably lower compared to the value obtained earlier for GST films (m = 90).[14]

Fragile-to-Strong Crossover. In the Angell plot, an Arrhenius behavior results in a fragility approaching ~15, such as holds for SiO_2,[46] categorized as a strong (supercooled) liquid (cf. Figure 4). Larger values of fragility lead to non-Arrhenius behavior, classified as fragile, such as has been presented for the GST films.[14] However, in some (undercooled) liquids a single fragility model is not able to describe the temperature dependence of viscosity. Then, the coexistence of Arrhenius behavior at low temperature and non-Arrhenius behavior at high temperature has been successfully explained by a fragile-to-strong (FS) crossover,[27] which is a ubiquitous feature in glass formers. First discovered in water,[49] this phenomenon has thereafter been observed in glass-forming liquids,[27] chalcogenides,[50,51] and Ag–In–Sb–Te PCMs.[20] For instance, Figure 4 portrays the experimental viscosity data for $Ge_{15}Te_{85}$ (black open triangles) at temperatures near T_g[48] and melting temperature (T_m),[47] fitted with the corresponding dashed curve utilizing eq 4, where a distinct FS crossover is illustrated. The FS crossover in $Ge_{15}Te_{85}$ is confirmed by another work employing the Adam–Gibbs equation to fit the viscosity.[51] For GST NPs, the FS crossover is likewise discerned, demonstrated by the red and blue solid curves in Figure 4. With the strong segment near T_g, the viscosity drops exponentially with the increment of temperature with an intermediate fragility (strong), whereas a further increase in temperature yields a nonexponential decline of viscosity (fragile). The FS crossover in GST NPs is weaker than that of $Ge_{15}Te_{85}$, where the two segments of viscosity are clearly distinguished. Still, as we explain in the next paragraph, there are strong arguments that the FS crossover actually occurs in GST NPs and that it is not a misinterpretation of a (more ordinary) glass transition.

A similar temperature dependence of the growth rate as in the present work was also observed for AgInSbTe PCMs, where the Arrhenius dependence of viscosity was found at lower temperatures, while the MYEGA model (non-Arrhenius dependence) was obtained at higher temperatures.[19,21] At that time it was proposed that the Arrhenius behavior correlates to the glassy state, whereas the non-Arrhenius behavior is associated with the supercooled liquid state. In this scenario, this divergence in temperature dependence of viscosity appears at the junction between glass and supercooled liquid. If our observed (FS transition) behavior is explained as a glass transition, that would lead to a T_g of ~438 K for GST NPs (H_2). Taking this value for T_g, we then obtain a viscosity at T_g of 10^3 Pa s. It is obvious that this viscosity is in conflict with the definition of glass transition temperature (where the viscosity is 10^{12} Pa s). Moreover, we also observed crystallization at a temperature about 20 K lower than this supposed T_g of ~438

DOI: 10.1021/acs.jpcc.6b11707
J. Phys. Chem. C 2017, 121, 8569–8578

K,[26] which is also inconsistent with the notation that crystallization is only possible above T_g. Clearly, with the fragile-to-strong crossover model, these conflicts are avoided. Therefore, the FS crossover is a more plausible explanation of our observations than the (supercooled liquid to) glass transition.

The present results therefore show the presence of the FS crossover, which already was signified by the large Arrhenius region shown in Figure 3b. It occurs for both samples approximately at 0.85 T_g/T, a T_g-scaled temperature lower than that of $Ge_{15}Te_{85}$ and AgInSbTe.[20] The CH_4 addition has negligible influence on this crossover. For GST films reported by Orava et al., however, the FS crossover was not observed, and a viscosity model with a single fragility value (Cohen and Grest model) was adopted to fit the Kissinger plot obtained through ultrafast DSC,[14] denoted as the black dotted curve in Figure 4. The high fragility of GST films results in a sharp reduction of viscosity at temperatures just above T_g. Yet, the lower fragility for GST NPs, caused by the FS crossover, yields a less acute decline in viscosity. Consequently, the GST NPs exhibit a higher viscosity at lower temperature in comparison to the GST films, as distinguished at ~0.9−1 T_g/T in Figure 4. These results thus suggest that NPs are advantageous in phase-change memory as higher viscosity correlates to lower atomic diffusivity and therefore longer data retention time.

In a previous work,[16] the growth rate of nitrogen-doped GST (N-GST) in memory cells was directly measured in a large temperature regime (from ~420 to ~530 K), where the overall growth rate of the N-GST deviates in temperature dependence: Arrhenius behavior at low temperature and non-Arrhenius behavior at high temperature. The experimental data for growth rate were transposed to viscosity using eq 2, with decoupling parameter ξ = 0.72 and other parameters (viz. T_m, r_{atom}, λ, and R_{hyd} in eq 2) from this article. ξ is adjusted to make $\eta(T_g)$ = 10^{12} Pa s, and this value of ξ is close to that for GST films reported previously.[14] The transposed viscosity is presented as blue stars in Figure 4. The MYEGA model for viscosity with one fragility cannot fit these data when specifying $\eta(T_m)$ as 1.2 × 10^{-3} Pa s.[52] In contrast, the generalized MYEGA model (eq 4) yields a good fit to the viscosity of N-GST, providing a strong indication that the FS crossover also occurs in these N-doped GST films employed in memory cells. In another work,[17] a similar temperature dependence in the growth rate of GST is observed, and two terms of temperature dependence were utilized to fit the Kissinger plot for GST confined in a memory cell. Yet, the FS crossover was not proposed to explain the observed behavior, but in light of the present work it has thus been generally observed for GST in memory cells.

It has been suggested that FS crossover exists only in growth-dominated PCMs but not in nucleation-dominated PCMs.[53] Melt-quenched GST PCMs confined in a cell are considered (by their nanoscale volume) as growth-dominated PCMs.[17] While GST films are considered as nucleation-dominated PCMs, GST NPs, on the other hand, also possess growth-dominated crystallization ascribed to the extremely small volume for crystallization caused by down-scaling. For instance, in our previous work we found by high-resolution TEM only single crystalline NPs.[26] Nevertheless, small crystal domains are generally expected for surface-induced heterogeneous nucleation dominated crystallization of GST PCMs.[54] However, the NPs in the present work are apparently that small that they still form single crystals. Therefore, it might be possible that the presence of the FS crossover in GST NPs compared to its absence in GST films can be attributed to the down-scaling induced change in the crystallization mechanism from nucleation dominant to growth dominant.

Overall Growth Rate of $Ge_2Sb_2Te_5$ Nanoparticles. The overall growth rate of the crystallization for the GST NPs is of technological relevance, e.g., for PC memories, as it is associated with data retention at the lower temperatures and the switching speed at higher temperatures. The blue and red solid curves in Figure 5 show the overall growth rate, as derived

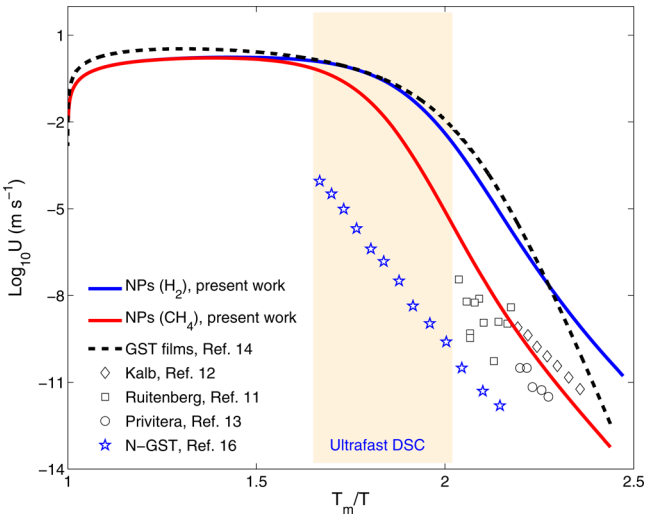

Figure 5. The growth rates of GST NPs between T_g and T_m. Blue and red curves represent the data for GST (H_2) and GST (CH_4), respectively. The black dashed curve is the growth rate for GST films,[14] while the black data points are from direct measurements via transmission electron microscopy[11,13] and atomic force microscopy.[12] The directly measured growth rate for nitrogen-doped GST films is also shown in this figure;[16] see the blue stars in this figure. The light yellow shaded area denotes the actual measurement regime accessed by ultrafast DSC.

using eq 2, ranging from T_g to T_m for both NPs (H_2) and NPs (CH_4), respectively. In comparison, the growth rate of GST films obtained by Orava et al. is also depicted as a black dashed curve in Figure 5.[14] The maximum growth rate (U_m) for these 2 types of NPs is very similar, 1.7 and 1.6 m s^{-1}, with U_m taking place at approximately 0.7 T/T_m. These values for NPs are reasonably close to U_m of GST films, as can be observed in Figure 5 by comparing the blue and red solid curves for the GST NPs with the black dashed curve holding for GST films. In a previous work, the growth rate of Ge−Sb alloy reaches a maximum value at ~0.9 T/T_m,[23] which is plausible, because the U_m of growth-dominated PCMs is considered to occur at a higher T/T_m compared to nucleation-dominated PCMs.[20]

Although the NPs (CH_4) possess a lower growth rate at lower temperature range (below 520 K), it coincides with the one for NPs (H_2) when the temperature is beyond 590 K. The lower growth rate for NPs (CH_4) at low temperature is similar to the retardation induced by carbon doping in GST films,[37] as carbon (a byproduct decomposed from methane in plasmas) is expected to be incorporated into the NPs. When the temperature becomes higher, the FS crossover appears, and then the fragile regime of viscosity is accessed. As a consequence, the viscosity strongly drops to equivalent values generating final convergence of the growth rates. This trend is also indicated by the viscosity in Figure 4, where the difference

DOI: 10.1021/acs.jpcc.6b11707
J. Phys. Chem. C 2017, 121, 8569−8578

is less apparent, because Figure 4 is normalized with respect to T_g. This makes the NPs (CH_4) preferable for PC memory application as lower growth rates at low temperatures associated with a higher activation energy indicate a longer data retention time; meanwhile, the still comparable growth rates at higher temperature enable sufficient rapid switching (to the crystalline SET state); see the more detailed discussion in Section 5 of the SI.

The growth rate undergoes an Arrhenius-like behavior at temperatures just above T_g, and non-Arrhenius behavior emerges with a further increase of temperature, demonstrating a temperature-dependent activation energy (E_g, derived from the gradient of this curve) for crystal growth during crystallization. With similar slopes to the independent data near T_g, the E_g is determined as ∼2.8 and ∼3.2 eV at^{-1} for the NPs (H_2) and NPs (CH_4), as can be seen in Figure S6. For $Ge_2Sb_2Te_5$ films it is well-established that the activation energy for crystallization and for growth near T_g is in the range 2.2−3.0 eV at^{-1}.[10−13,36,55] In comparison, the growth rate of GST films derived in ref 14 presents a considerably higher activation energy, ∼5.0 eV at^{-1} near T_g, which appears unrealistic. Although a high fragility of the GST thin film can lead to a high activation energy, this fragility was obtained fully through modeling and fitting and not based on any directly measured data, inferring that the high fragility for the thin film could be erroneous.

However, it is still evident that the growth rates for the NPs (H_2) observed in the present work exhibit a large gap (∼2 orders of magnitude) with the directly measured data obtained for GST films (open black data points in Figure 5).[11−13] This discrepancy can have several origins, e.g.: (1) The NPs (H_2) crystallize at lower temperature than films, leading to a faster growth rate at the same temperature. The NPs (CH_4) represent an evidently lower growth rate at the same temperature compared to NPs (H_2) due to the increase of T_p. Similarly, the nitrogen-doped GST films (confined in memory cells) even show smaller growth rate than GST films,[16] as demonstrated by the blue stars in Figure 5. (2) The constant nuclei density hypothesis that was adopted in JMAK modeling is over-simplified and may result in an erroneous fitting of the data in the Kissinger plot and therefore may cause a considerable shift to higher growth rates at the lower temperatures. However, several clearly more advanced models for nucleation were also tested, and these models did not significantly reduce the gap between the growth rates derived for the NPs (H_2) (blue solid line in Figure 5) and the directly measured data obtained for GST films (black open data points in Figure 5); for more details see the SI and in particular Figure S7.

CONCLUSIONS

Ultrafast differential scanning calorimetry has been employed to investigate the crystallization kinetics of $Ge_2Sb_2Te_5$ phase-change nanoparticles (NPs) synthesized by gas-phase condensation. The NPs show a relatively narrow size distribution around an average diameter of ∼16 nm. Varying the heating rate during the DSC measurements with 3 orders of magnitude, it is observed that (1) the crystallization rate complies with Arrhenius behavior within an (unexpectedly) large temperature range directly above T_g (for T_g/T values from 0.85 to 1) and (2) a non-Arrhenius fragile behavior occurs at higher temperatures (for T_g/T values lower than 0.85). This unique feature can be explained well (only) by utilizing a fragile-to-strong crossover model for the viscosity, from which the overall viscosity and growth rate of the NPs have been derived. This crossover is clearly observed here for the $Ge_2Sb_2Te_5$ NPs, while it was not observed earlier for GST films. This enables NPs to have both longer data retention times at low temperatures and high switching speed at high temperatures, entailing the NPs to be an advantageous contender in phase-change materials based devices. Moreover, it is demonstrated that CH_4 incorporation during the NP production reduces the crystal growth rate by about 2 orders of magnitude at lower temperatures and thus improves the data retention, whereas the maximum growth rate remains unchanged. This positive "doping" effect makes $Ge_2Sb_2Te_5$ NPs even more suitable candidates for phase-change memory applications.

ASSOCIATED CONTENT

Supporting Information

The Supporting Information is available free of charge on the ACS Publications website at DOI: 10.1021/acs.jpcc.6b11707.

Figures showing the size distribution and composition of the nanoparticles, the image of the sample, the influence of sample on the crystallization, fits with different viscosity models, the activation energy for crystal growth,and the fits with other nucleation models (PDF)

AUTHOR INFORMATION

Corresponding Author

*E-mail: b.j.kooi@rug.nl.

ORCID

Bin Chen: 0000-0003-1591-0843

Author Contributions

The manuscript was written through contributions of all authors. All authors have given approval to the final version of the manuscript.

Notes

The authors declare no competing financial interest.

ACKNOWLEDGMENTS

We gratefully acknowledge the China Scholarship Council for financial support (of B.C.).

REFERENCES

(1) Wuttig, M. Phase-Change Materials: Towards a Universal Memory? *Nat. Mater.* **2005**, *4* (4), 265−266.

(2) Wuttig, M.; Yamada, N. Phase-Change Materials for Rewriteable Data Storage. *Nat. Mater.* **2007**, *6* (11), 824−832.

(3) Raoux, S.; Welnic, W.; Ielmini, D. Phase Change Materials and Their Application to Nonvolatile Memories. *Chem. Rev.* **2010**, *110* (1), 240−267.

(4) Hosseini, P.; Wright, C. D.; Bhaskaran, H. An Optoelectronic Framework Enabled by Low-Dimensional Phase-Change Films. *Nature* **2014**, *511* (7508), 206−211.

(5) Waldecker, L.; Miller, T. A.; Rudé, M.; Bertoni, R.; Osmond, J.; Pruneri, V.; Simpson, R. E.; Ernstorfer, R.; Wall, S. Time-Domain Separation of Optical Properties from Structural Transitions in Resonantly Bonded Materials. *Nat. Mater.* **2015**, *14* (10), 991−995.

(6) Burr, G. W.; Shelby, R. M.; Sidler, S.; Nolfo, C. di; Jang, J.; Boybat, I.; Shenoy, R. S.; Narayanan, P.; Virwani, K.; Giacometti, E. U.; et al. Experimental Demonstration and Tolerancing of a Large-Scale Neural Network (165 000 Synapses) Using Phase-Change Memory as the Synaptic Weight Element. *IEEE Trans. Electron Devices* **2015**, *62* (11), 3498−3507.

DOI: 10.1021/acs.jpcc.6b11707
J. Phys. Chem. C 2017, 121, 8569−8578

(7) Tuma, T.; Pantazi, A.; Le Gallo, M.; Sebastian, A.; Eleftheriou, E. Stochastic Phase-Change Neurons. *Nat. Nanotechnol.* **2016**, *11*, 693.
(8) Ríos, C.; Stegmaier, M.; Hosseini, P.; Wang, D.; Scherer, T.; Wright, C. D.; Bhaskaran, H.; Pernice, W. H. P. Integrated All-Photonic Non-Volatile Multi-Level Memory. *Nat. Photonics* **2015**, *9* (11), 725−732.
(9) Rudé, M.; Simpson, R. E.; Quidant, R.; Pruneri, V.; Renger, J. Active Control of Surface Plasmon Waveguides with a Phase Change Material. *ACS Photonics* **2015**, *2* (6), 669−674.
(10) Friedrich, I.; Weidenhof, V.; Njoroge, W.; Franz, P.; Wuttig, M. Structural Transformations of $Ge_2Sb_2Te_5$ Films Studied by Electrical Resistance Measurements. *J. Appl. Phys.* **2000**, *87* (9), 4130−4134.
(11) Ruitenberg, G.; Petford-Long, A. K.; Doole, R. C. Determination of the Isothermal Nucleation and Growth Parameters for the Crystallization of Thin $Ge_2Sb_2Te_5$ Films. *J. Appl. Phys.* **2002**, *92* (6), 3116−3123.
(12) Kalb, J.; Spaepen, F.; Wuttig, M. Atomic Force Microscopy Measurements of Crystal Nucleation and Growth Rates in Thin Films of Amorphous Te Alloys. *Appl. Phys. Lett.* **2004**, *84* (25), 5240−5242.
(13) Privitera, S.; Bongiorno, C.; Rimini, E.; Zonca, R. Crystal Nucleation and Growth Processes in $Ge_2Sb_2Te_5$. *Appl. Phys. Lett.* **2004**, *84* (22), 4448−4450.
(14) Orava, J.; Greer, A. L.; Gholipour, B.; Hewak, D. W.; Smith, C. E. Characterization of Supercooled Liquid $Ge_2Sb_2Te_5$ and Its Crystallization by Ultrafast-Heating Calorimetry. *Nat. Mater.* **2012**, *11* (4), 279−283.
(15) Ciocchini, N.; Cassinerio, M.; Fugazza, D.; Ielmini, D. Evidence for Non-Arrhenius Kinetics of Crystallization in Phase Change Memory Devices. *IEEE Trans. Electron Devices* **2013**, *60* (11), 3767−3774.
(16) Sebastian, A.; Le Gallo, M.; Krebs, D. Crystal Growth within a Phase Change Memory Cell. *Nat. Commun.* **2014**, DOI: 10.1038/ncomms5314.
(17) Jeyasingh, R.; Fong, S. W.; Lee, J.; Li, Z.; Chang, K.-W.; Mantegazza, D.; Asheghi, M.; Goodson, K. E.; Wong, H.-S. P. Ultrafast Characterization of Phase-Change Material Crystallization Properties in the Melt-Quenched Amorphous Phase. *Nano Lett.* **2014**, *14* (6), 3419−3426.
(18) Santala, M. K.; Reed, B. W.; Raoux, S.; Topuria, T.; LaGrange, T.; Campbell, G. H. Irreversible Reactions Studied with Nanosecond Transmission Electron Microscopy Movies: Laser Crystallization of Phase Change Materials. *Appl. Phys. Lett.* **2013**, *102* (17), 174105.
(19) Salinga, M.; Carria, E.; Kaldenbach, A.; Bornhöfft, M.; Benke, J.; Mayer, J.; Wuttig, M. Measurement of Crystal Growth Velocity in a Melt-Quenched Phase-Change Material. *Nat. Commun.* **2013**, DOI: 10.1038/ncomms3371.
(20) Orava, J.; Hewak, D. W.; Greer, A. L. Fragile-to-Strong Crossover in Supercooled Liquid Ag-In-Sb-Te Studied by Ultrafast Calorimetry. *Adv. Funct. Mater.* **2015**, *25* (30), 4851−4858.
(21) Zalden, P.; von Hoegen, A.; Landreman, P.; Wuttig, M.; Lindenberg, A. M. How Supercooled Liquid Phase-Change Materials Crystallize: Snapshots after Femtosecond Optical Excitation. *Chem. Mater.* **2015**, *27* (16), 5641−5646.
(22) Eising, G.; Van Damme, T.; Kooi, B. J. Unraveling Crystal Growth in GeSb Phase-Change Films in between the Glass-Transition and Melting Temperatures. *Cryst. Growth Des.* **2014**, *14* (7), 3392−3397.
(23) Chen, B.; Momand, J.; Vermeulen, P. A.; Kooi, B. J. Crystallization Kinetics of Supercooled Liquid Ge−Sb Based on Ultrafast Calorimetry. *Cryst. Growth Des.* **2016**, *16* (1), 242−248.
(24) Lee, S.-H.; Jung, Y.; Agarwal, R. Highly Scalable Non-Volatile and Ultra-Low-Power Phase-Change Nanowire Memory. *Nat. Nanotechnol.* **2007**, *2* (10), 626−630.
(25) Xiong, F.; Liao, A. D.; Estrada, D.; Pop, E. Low-Power Switching of Phase-Change Materials with Carbon Nanotube Electrodes. *Science* **2011**, *332* (6029), 568−570.
(26) Chen, B.; ten Brink, G. H.; Palasantzas, G.; Kooi, B. J. Size-Dependent and Tunable Crystallization of GeSbTe Phase-Change Nanoparticles. *Sci. Rep.* **2016**, DOI: 10.1038/srep39546.
(27) Zhang, C.; Hu, L.; Yue, Y.; Mauro, J. C. Fragile-to-Strong Transition in Metallic Glass-Forming Liquids. *J. Chem. Phys.* **2010**, *133* (1), 014508.
(28) Wei; Xiaoqian; Shi; Luping; Chong; Chong, T.; Zhao; Rong; Lee; Koon, H. Thickness Dependent Nano-Crystallization in $Ge_2Sb_2Te_5$ Films and Its Effect on Devices. *Jpn. J. Appl. Phys.* **2007**, *46* (4S), 2211.
(29) Kalb, J. a.; Wuttig, M.; Spaepen, F. Calorimetric Measurements of Structural Relaxation and Glass Transition Temperatures in Sputtered Films of Amorphous Te Alloys Used for Phase Change Recording. *J. Mater. Res.* **2007**, *22* (03), 748−754.
(30) Roorda, S.; Doorn, S.; Sinke, W. C.; Scholte, P. M. L. O.; van Loenen, E. Calorimetric Evidence for Structural Relaxation in Amorphous Silicon. *Phys. Rev. Lett.* **1989**, *62* (16), 1880−1883.
(31) Donovan, E. P.; Spaepen, F.; Turnbull, D.; Poate, J. M.; Jacobson, D. C. Calorimetric Studies of Crystallization and Relaxation of Amorphous Si and Ge Prepared by Ion Implantation. *J. Appl. Phys.* **1985**, *57* (6), 1795−1804.
(32) Kissinger, H. E. Reaction Kinetics in Differential Thermal Analysis. *Anal. Chem.* **1957**, *29* (11), 1702−1706.
(33) Yamada, N.; Ohno, E.; Nishiuchi, K.; Akahira, N.; Takao, M. Rapid-phase Transitions of GeTe-Sb_2Te_3 Pseudobinary Amorphous Thin Films for an Optical Disk Memory. *J. Appl. Phys.* **1991**, *69* (5), 2849−2856.
(34) Ohshima, N. Crystallization of Germanium−antimony−tellurium Amorphous Thin Film Sandwiched between Various Dielectric Protective Films. *J. Appl. Phys.* **1996**, *79* (11), 8357−8363.
(35) Kim, Y.; Park, S. A.; Baeck, J. H.; Noh, M. K.; Jeong, K.; Cho, M.-H.; Park, H. M.; Lee, M. K.; Jeong, E. J.; Ko, D.-H.; et al. Phase Separation of a $Ge_2Sb_2Te_5$ Alloy in the Transition from an Amorphous Structure to Crystalline Structures. *J. Vac. Sci. Technol., A* **2006**, *24* (4), 929−933.
(36) Tominaga, J.; Shima, T.; Fons, P.; Simpson, R.; Kuwahara, M.; Kolobov, A. What Is the Origin of Activation Energy in Phase-Change Film? *Jpn. J. Appl. Phys.* **2009**, *48* (3S1), 03A053.
(37) Zhou, X.; Wu, L.; Song, Z.; Rao, F.; Zhu, M.; Peng, C.; Yao, D.; Song, S.; Liu, B.; Feng, S. Carbon-Doped Ge2Sb2Te5 Phase Change Material: A Candidate for High-Density Phase Change Memory Application. *Appl. Phys. Lett.* **2012**, *101* (14), 142104.
(38) Thompson, C. V.; Spaepen, F. On the Approximation of the Free Energy Change on Crystallization. *Acta Metall.* **1979**, *27* (12), 1855−1859.
(39) Kalb, J. A.; Wuttig, M. Crystallization Kinetics in Antimony and Tellurium Alloys Used for Phase Change Recording 10.02.2006. Publikationsserver der RWTH Aachen University, 2006.
(40) Ediger, M. D. Spatially Heterogeneous Dynamics in Supercooled Liquids. *Annu. Rev. Phys. Chem.* **2000**, *51* (1), 99−128.
(41) Mauro, J. C.; Yue, Y.; Ellison, A. J.; Gupta, P. K.; Allan, D. C. Viscosity of Glass-Forming Liquids. *Proc. Natl. Acad. Sci. U. S. A.* **2009**, *106* (47), 19780−19784.
(42) Cohen, M. H.; Grest, G. S. Liquid-Glass Transition, a Free-Volume Approach. *Phys. Rev. B: Condens. Matter Mater. Phys.* **1979**, *20* (3), 1077−1098.
(43) Wang, L.-M.; Mauro, J. C. An Upper Limit to Kinetic Fragility in Glass-Forming Liquids. *J. Chem. Phys.* **2011**, *134* (4), 044522.
(44) Morales-Sánchez, E.; Prokhorov, E. F.; Mendoza-Galván, A.; González-Hernández, J. Determination of the Glass Transition and Nucleation Temperatures in $Ge_2Sb_2Te_5$ Sputtered Films. *J. Appl. Phys.* **2002**, *91* (2), 697−702.
(45) Cho, J.-Y.; Kim, D.; Park, Y.-J.; Yang, T.-Y.; Lee, Y.-Y.; Joo, Y.-C. The Phase-Change Kinetics of Amorphous $Ge_2Sb_2Te_5$ and Device Characteristics Investigated by Thin-Film Mechanics. *Acta Mater.* **2015**, *94*, 143−151.
(46) Angell, C. A. Formation of Glasses from Liquids and Biopolymers. *Science* **1995**, *267* (5206), 1924−1935.
(47) Neumann, H.; Herwig, F.; Hoyer, W. The Short Range Order of Liquid Eutectic AIII-Te and AIV-Te Alloys. *J. Non-Cryst. Solids* **1996**, *205*−*207* (Part 1), 438−442.

DOI: 10.1021/acs.jpcc.6b11707
J. Phys. Chem. C 2017, 121, 8569−8578

(48) Rocca, J.; Erazú, M.; Fontana, M.; Arcondo, B. Crystallization Process on Amorphous GeTeSb Samples near to Eutectic Point $Ge_{15}Te_{85}$. *J. Non-Cryst. Solids* **2009**, *355* (37−42), 2068−2073.
(49) Ito, K.; Moynihan, C. T.; Angell, C. A. Thermodynamic Determination of Fragility in Liquids and a Fragile-to-Strong Liquid Transition in Water. *Nature* **1999**, *398* (6727), 492−495.
(50) Stølen, S.; Grande, T.; Johnsen, H.-B. Fragility Transition in $GeSe_2$ − Se Liquids. *Phys. Chem. Chem. Phys.* **2002**, *4* (14), 3396−3399.
(51) Wei, S.; Lucas, P.; Angell, C. A. Phase Change Alloy Viscosities down to Tg Using Adam-Gibbs-Equation Fittings to Excess Entropy Data: A Fragile-to-Strong Transition. *J. Appl. Phys.* **2015**, *118* (3), 034903.
(52) Akola, J.; Jones, R. O. Structural Phase Transitions on the Nanoscale: The Crucial Pattern in the Phase-Change Materials $Ge_2Sb_2Te_5$ and GeTe. *Phys. Rev. B: Condens. Matter Mater. Phys.* **2007**, *76* (23), 235201.
(53) Orava, J.; Weber, H.; Kaban, I.; Greer, A. L. Viscosity of Liquid Ag−In−Sb−Te: Evidence of a Fragile-to-Strong Crossover. *J. Chem. Phys.* **2016**, *144* (19), 194503.
(54) Lee, S.-H.; Jung, Y.; Agarwal, R. Size-Dependent Surface-Induced Heterogeneous Nucleation Driven Phase-Change in $Ge_2Sb_2Te_5$ Nanowires. *Nano Lett.* **2008**, *8* (10), 3303−3309.
(55) Redaelli, A.; Pirovano, A.; Tortorelli, I.; Ielmini, D.; Lacaita, A. L. A Reliable Technique for Experimental Evaluation of Crystallization Activation Energy in PCMs. *IEEE Electron Device Lett.* **2008**, *29* (1), 41−43.

DOI: 10.1021/acs.jpcc.6b11707
J. Phys. Chem. C 2017, 121, 8569−8578